Journal of Science and Technology in Civil Engineering, HUCE, 2023, 17 (3): 21–32

EFFECT OF TEMPERATURE ON ELECTRICAL RESISTIVITY OF HIGH-PERFORMANCE FIBER-REINFORCED CONCRETES

Phan Tan Duy[a,b], Le Ba Khanh[a,b], Nguyen Duy Liem[c,*], Nguyen Van Thuan[d]

[a]*Faculty of Civil Engineering, Ho Chi Minh City University of Technology, 268 Ly Thuong Kiet street, District 10, Ho Chi Minh city, Vietnam*
[b]*Vietnam National University Ho Chi Minh City, Linh Trung ward, Thu Duc city, Ho Chi Minh city, Vietnam*
[c]*Faculty of Civil Engineering, Ho Chi Minh City University of Technology and Education, 01 Vo Van Ngan street, Thu Duc city, Ho Chi Minh city, Vietnam*
[d]*Faculty of Traffic Engineering, Nha Trang University, 02 Nguyen Dinh Chieu street, Nha Trang city, Khanh Hoa province, Vietnam*

Article history:
Received 10/4/2023, Revised 07/6/2023, Accepted 14/6/2023

Abstract

The effect of temperature on the electrical resistivity of high-performance fiber-reinforced concretes (HPFRCs) was highlighted in this investigation through an experimental approach. There are four HPFRC mixtures as follows: HPFRC0 (no fiber), HPFRC1 (macro steel fiber, 1.5% by volume), HPFRC2 (micro steel fiber, 1.5% by volume), and HPFRC3 (hybrid fiber, 1.0% macro steel fiber blended with 0.5% micro steel fiber). All HPFRC specimens had an identical size of 40 × 40 × 160 mm^3 (width × depth × length). The electrical resistivity of HPFRCs was measured under three temperature levels, including 0 °C, 25 °C, and 50 °C using a chamber machine. The research proved that the electrical resistivity of the studied HPFRCs obviously decreased with increasing the temperature ranging from 0 °C to 50 °C. Generally, the temperature exhibited a considerable effect on the electrical resistivities of cement-based composites.

Keywords: temperature; electrical resistivity; high-performance fiber-reinforced concrete; smart material.

https://doi.org/10.31814/stce.huce2023-17(3)-02

1. Introduction

Since the breakdown of the Morandi Bridge in Italy happened in 2018, structural health monitoring (SHM) has played a very essential role to prevent catastrophic structural breakdown. Currently, the SHM approach commonly employs attached and/or embedded sensors into the structural member to monitor the structural response and then evaluate the structural properties in terms of load-carrying capability and service life [1, 2]. Fig. 1 shows the schematic of a typical SHM system in a bridge structure. As can be seen in Fig. 1, a typical SHM system comprises three main parts as follows: a sensor network, a data processing system, and a health evaluation method for decision-making. The current SHM approach has been still disadvantageous in the monitoring work, such as high cost, low durability, and limited sensing area of the common sensors [3]. Moreover, the embedding of sensors into a structure may be the main reason leading to a decrease in the load-carrying capacity of the structure. To overcome these limitations of the present SHM systems, a new approach is proposed employing smart construction material with self-sensing capacity for monitoring work. For operating mechanisms, the smart materials can themselves sense or respond to structural strain (stress) and damage (cracks) based on the electrical resistivity of these materials under external loads [4, 5].

High-performance fiber-reinforced concrete (HPFRC) has recently been claimed as a superior building material because it exhibits great compressive, flexural, and tensile resistance as well as

*Corresponding author. *E-mail address:* liemnd@hcmute.edu.vn (Nguyen, D. L.)

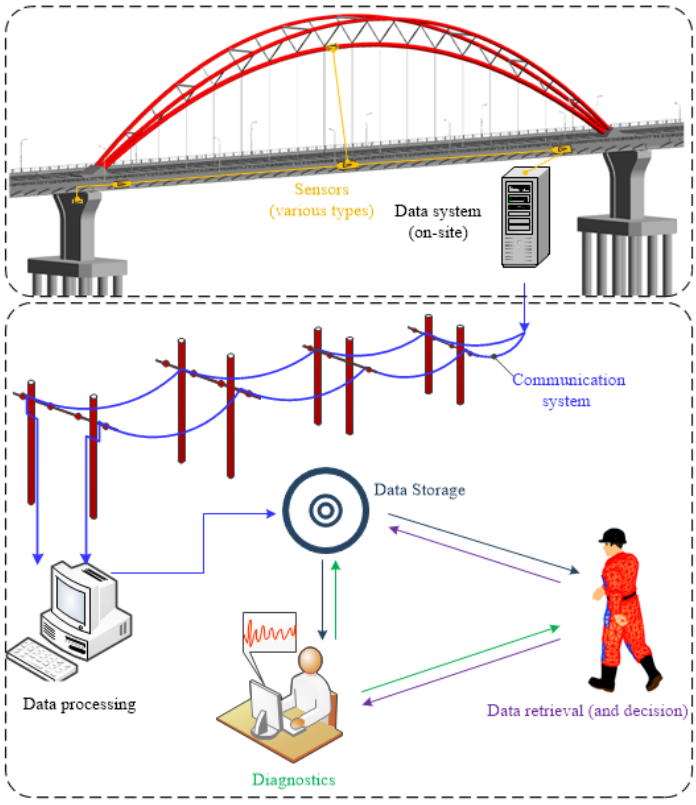

Figure 1. Illustration of a common SHM system for a bridge structure

excellent ductility and toughness under external loads [6–10]. Along with the outstanding properties mentioned above, HPFRC materials may also have smart properties like self-healing [11] and self-strain/damage sensing [12–16]. As a result, the HPFRCs were categorized as smart or multifunctional materials [17]. For self-strain/damage sensing of HPFRCs, the stress, strain, or damage of HPFRCs can be simply derived by measuring their electrical resistivity, with no requirement of additional sensors like SHM's conventional technique. It is obvious that electrical resistivity is an important parameter that strongly influences the self-sensing capacity of a material. For that reason, environmental factors, such as temperature, relative humidity, and others affecting the electrical resistivity of HPFRCs, should be investigated. In this study, we aim to experimentally investigate the effect of temperature on the electrical resistivity of HPFRCs. It is expected that the study findings will provide useful information for developing and utilizing the self-sensing characteristic of HPFRCs.

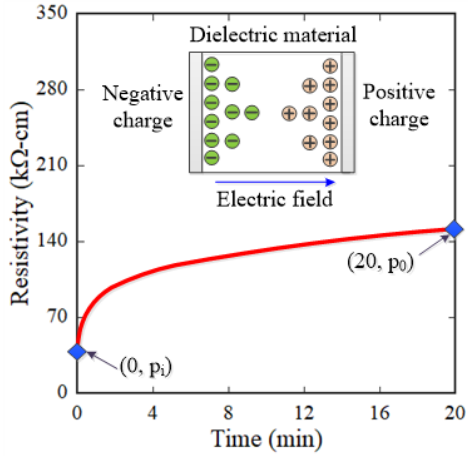

Figure 2. Typical electrical resistivity behavior of a cementitious composite owing to electrical polarization

2. Typical electrical resistivity behavior of cementitious composites

Fig. 2 shows the typical electrical resistivity behavior of a cementitious composite owing to electrical polarization [18–20]. The electrical polarization refers to the separation of the center of positive charge and the center of negative charge in a cementitious composite under a direct current (DC) electrical field [21]. In detail, when an electric field is applied, a net electric dipole moment is created, and this is known as the electrical polarization effect in materials. The electrical polarization happens within cement as well as at the interface between cement and electrical contact. As can be seen from Fig. 2, the electrical resistivity significantly increases in the early period but more and more slightly increases with time [12]. In this behavior, two parameters, including the initial resistivity at 0 min (ρ_i) and the stable resistivity at t_0 = 20 min (ρ_0) were experimentally investigated.

3. Experimental campaign

3.1. Materials and specimen preparation

Fig. 3 displays the layout of the experimental testing program of HPFRCs. As can be seen from Fig. 3, there were four types of HPFRCs with different steel fiber types and volume contents as follows: HPFRC0 (no fiber), HPFRC1 (macro fiber 1.5%), HPFRC2 (micro fiber 1.5%), and HPFRC3 (hybrid fiber including 1.0% macro fiber blended with 0.5% micro fiber. Table 1 provides the composition and compressive strength of the plain HPFRC matrix. Table 2 summarizes the features of the two types of steel fiber used in this research, and their photos were shown in Fig. 4. According to Table 2, the two types of steel fiber had their length/diameter ratio as follows: 35/0.5 for macro fiber and 13/0.2 for micro fiber. Among steel fiber characteristics, fiber length and aspect ratio were adopted to strongly influence concrete performance at fresh and hardened states [7, 12]. In this research work, we investigated two steel fibers as follows: 35/0.5 for macro fiber and 13/0.2 for micro fiber. These steel fiber types had nearly the same aspect ratios but greatly different lengths, which may produce a distinctive HPFRC performance, besides, both of them have been widely employed in Vietnam. All HPFRC specimens were prism-shaped with the same size of 40 × 40 × 160 mm. The mixing detail of HPFRC mixture could be referred to in the published document [9].

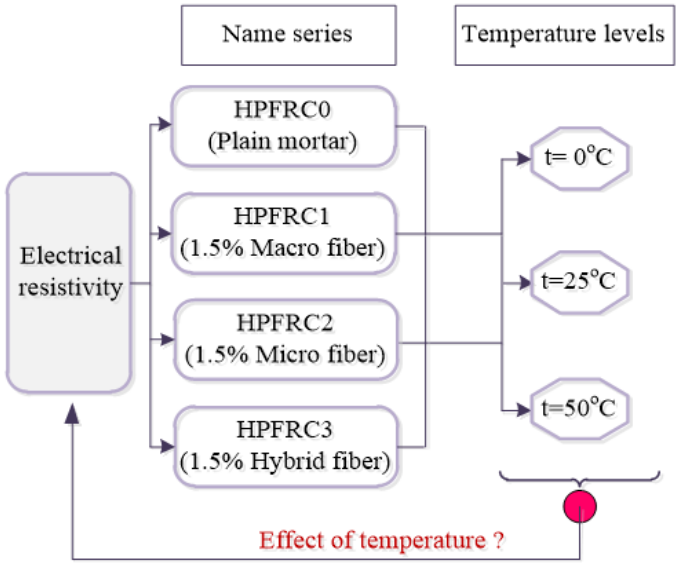

Figure 3. Layout of testing program

Table 1. Composition & compressive strength of mortar matrix

Component	Value
Cement	0.80
Silica fume	0.07
Silica sand	1.00
Fly ash	0.20
Superplas-ticizer	0.04
Water	0.26
Compressive strength (MPa)	72.00

Table 2. Properties of fibers used

Fiber type	Macro fiber	Micro fiber
Diameter (mm)	0.5	0.2
Length (mm)	35	13
Aspect ratio (Length/Diameter)	70	65
Density (g/cm^3)	7.9	7.9
Tensile strength (MPa)	> 1.200	> 2.500
Section form	Circular, hooked	Circular, smooth
Product origin	Vietnam	Vietnam

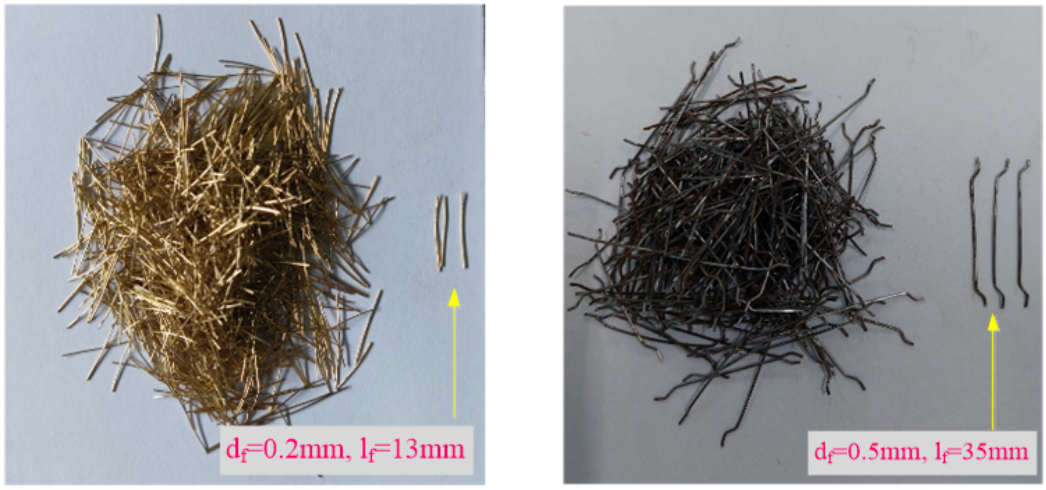

(a) Microfiber (b) Macrofiber

Figure 4. Picture of fibers used

After casting, all HPFRC specimens were placed in the laboratory room for 48 hours before demolding. After demolding, the HPFRC specimens were water-cured at the temperature from 22 °C to 29 °C for 28 days. Finally, the specimens were moved out from the water tank, then dried at laboratory temperature. In order to measure the electrical resistivity of the HPFRC specimens, the specimen was attached with four electrodes. At each electrode, a layer of electrical conductive-paste was firstly smeared onto the specimen surfaces to increase the electrical conductivity between the copper tapes and the specimens, as shown in Fig. 5. As the electric conductive-paste layer became dry, the copper

tape was attached to the electric conductive-paste layer onto the surface of the specimen. The distance between the two outer current electrodes is 100 mm, while the distance between the two inner voltage electrodes is 60 mm. The specimens were tested at the age of approximately 30 days. At least three specimens of each HPFRC series were examined.

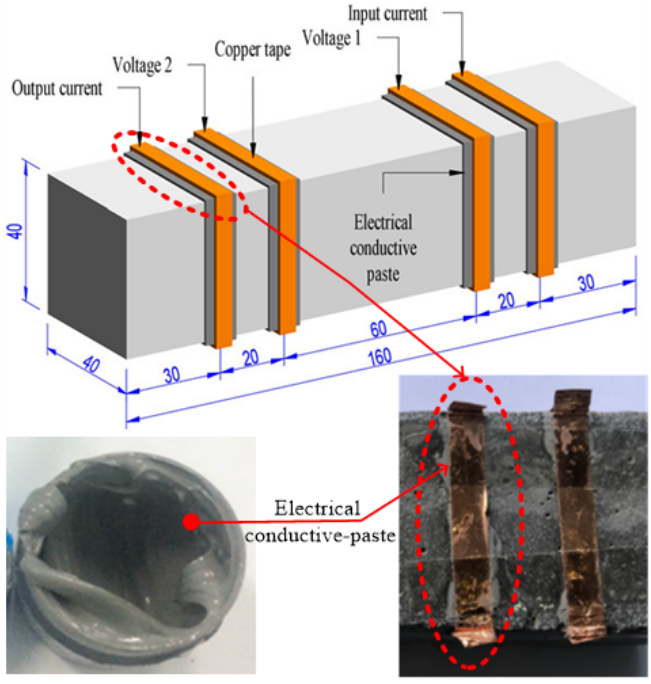

Figure 5. Preparation of tested specimen

3.2. Experiment setup

Fig. 6 shows the test setup for measuring electrical resistances of HPFRC specimens in this research. There were four specimens placed in a chamber that can control temperatures ranging from

(a) Photo of chamber used

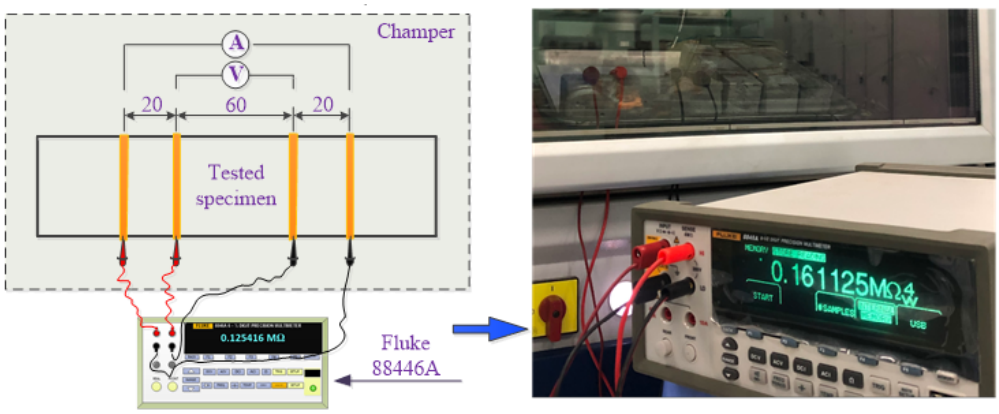

(b) Machine scheme for measuring electrical resistance

Figure 6. Test setup for measuring the electrical resistance of HPFRCs

−15 °C to +120 °C, as illustrated in Fig. 6(a). The Fluke 8846A multimeter was employed to measure the electrical resistance of the HPFRC specimen, as displayed in Fig. 6(b). Three temperature levels, including 0 °C, 25 °C, and 50 °C were designed to explore the effect of temperature on the electrical resistivity of HPFRCs. The humidity was kept at 70%. The measured electrical resistance of HPFRCs would be modified to electrical resistivity (ρ) using Eq. (1).

$$\rho = R \cdot \frac{F}{L} \tag{1}$$

where ρ denotes the electrical resistivity of a material; R represents the electrical resistance of a material; F and L are the cross-sectional area and the length between the two inner electrodes, respectively.

4. Test result and discussion

4.1. Electrical resistivity behavior of HPFRC under various temperature

Figs. 7–10 display the electrical resistivity versus time response curves of four studied HPFRC series: HPFRC0 (Fig. 7), HPFRC1 (Fig. 8), HPFRC2 (Fig. 9), and HPFRC3 (Fig. 10). Each figure was performed with three levels of temperature under DC electrical field. The curves of electrical resistivity versus time of all HPFRC series are generally consistent, regardless of the temperature

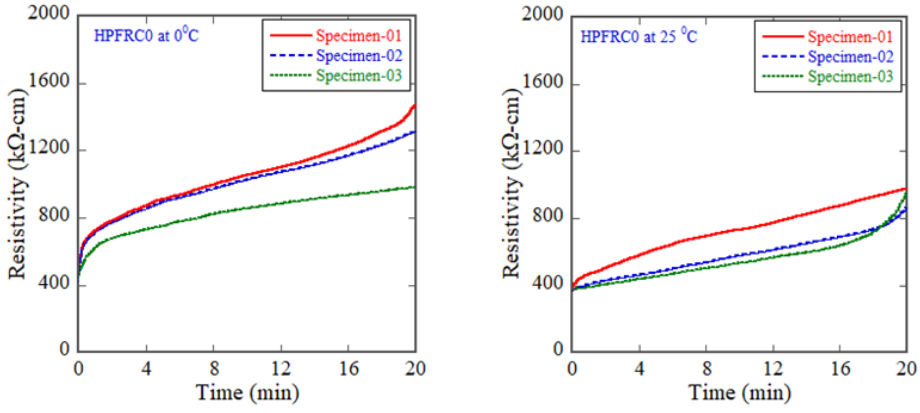

(a) At 0 °C (b) At 25 °C

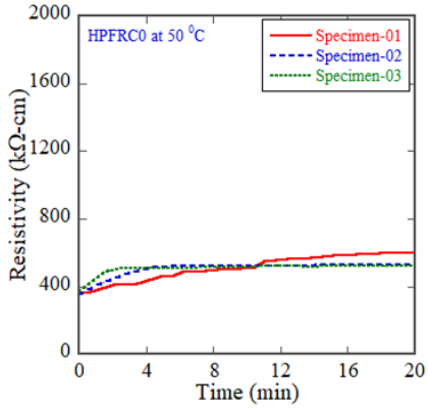

(c) At 50 °C

Figure 7. Electrical resistivity behavior of HPFRC0 under various temperature level

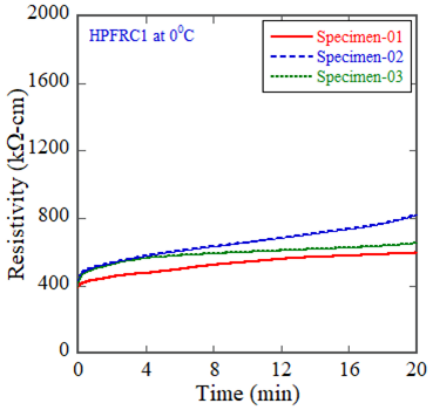

(a) At 0 °C

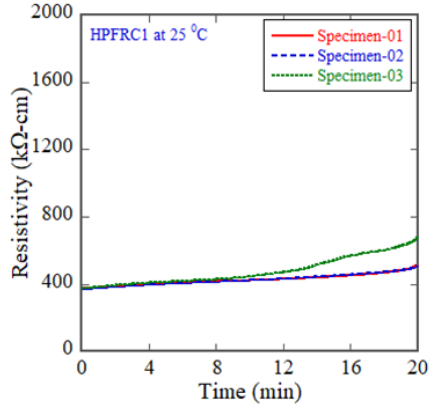

(b) At 25 °C

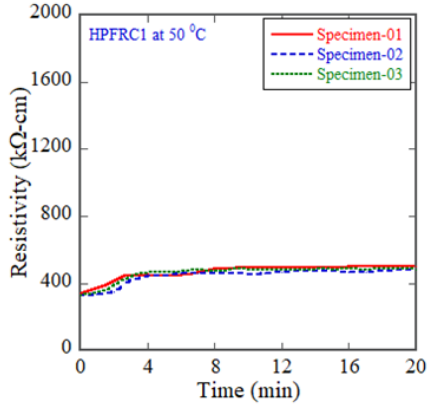

(c) At 50 °C

Figure 8. Electrical resistivity behavior of HPFRC1 under various temperature level

level. Also, the electrical polarizations are obvious with significant difference between ρ_i and ρ_0 in all the three cases of temperature. The most and least significant polarizations of the studied HPFRCs are observed at 0 °C and 50 °C, respectively. The average values and standard deviations of ρ_i and

ρ_0 were summarized in Table 3. The increase in electrical resistivity of HPFRCs with time under DC electrical field was completely agreed with those from the previous published documents [12–15]. Kim et al. [16] also confimed this phenomenon for of ultra-high-performance fiber-reinforced concretes (UHPFRCs), another type of HPFRCs.

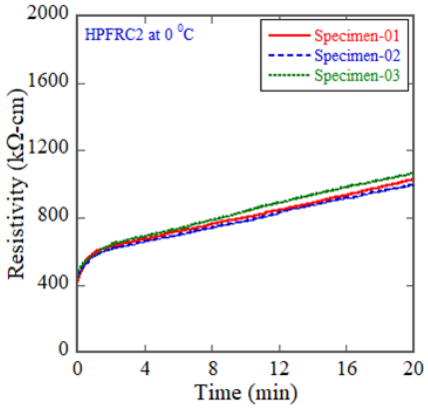

(a) At 0 °C

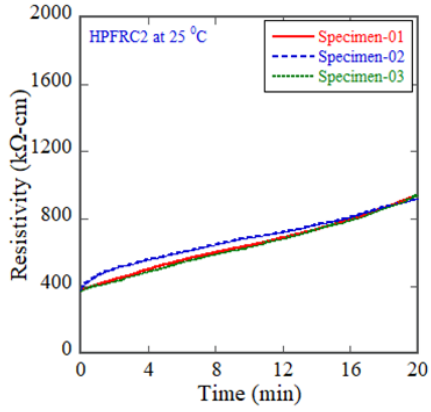

(b) At 25 °C

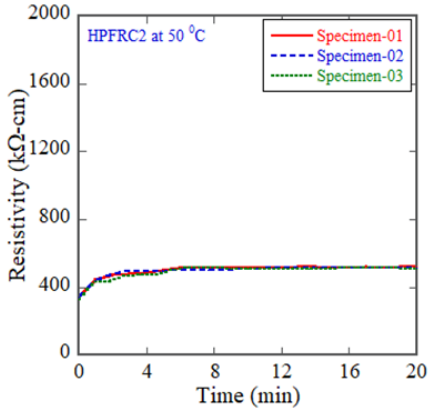

(c) At 50 °C

Figure 9. Electrical resistivity behavior of HPFRC2 under various temperature level

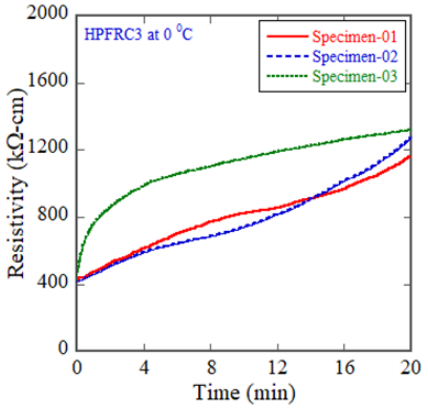

(a) At 0 °C

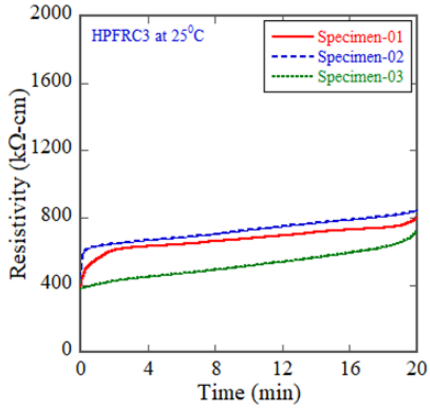

(b) At 25 °C

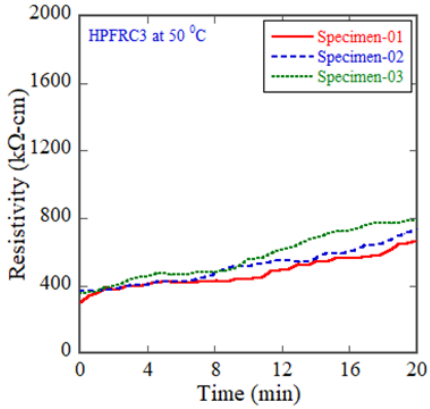

(c) At 50 °C

Figure 10. Electrical resistivity behavior of HPFRC3 under various temperature level

Table 3. Electrical resistivity of studied HPFRCs regarding temperature

Temp. level	Specimen	Series							
		HPFRC0		HPFRC1		HPFRC2		HPFRC3	
		ρ_i ($k\Omega$-cm)	ρ_0 ($k\Omega$-cm)	ρ_i ($k\Omega$-cm)	ρ_0 ($k\Omega$-cm)	ρ_i ($k\Omega$-cm)	ρ_0 ($k\Omega$-cm)	ρ_i ($k\Omega$-cm)	ρ_0 ($k\Omega$-cm)
0 °C	SP1	422.8	1474.5	386.6	594.7	417.8	1027.7	423.0	1161.1
	SP2	449.9	1408.7	395.0	822.8	449.0	994.4	416.8	1277.2
	SP3	423.5	1668.5	393.5	652.6	422.7	1064.5	427.0	1319.7
	Average value	432.1	1517.2	391.7	690.0	429.8	1028.9	422.3	1252.6
	Standard deviation	15.4	135.1	4.5	118.6	16.8	35.0	5.1	82.1
25 °C	SP1	364.9	976.6	371.9	515.8	372.1	939.9	375.4	812.6
	SP2	370.7	865.3	368.2	511.0	374.4	917.9	444.9	846.1
	SP3	374.9	963.1	372.1	682.0	371.9	941.5	378.9	717.9
	Average value	370.20	935.0	370.7	569.6	372.8	933.1	399.7	792.2
	Standard deviation	5.01	60.8	2.2	97.4	1.4	13.2	39.1	66.5
50 °C	SP1	361.1	597.7	343.8	503.2	339.4	519.7	296.5	665.9
	SP2	355.9	528.1	325.7	476.9	344.6	514.8	366.2	734.8
	SP3	370.5	527.0	324.3	480.7	325.1	509.9	351.7	793.2
	Average value	362.5	550.9	331.3	486.9	336.4	514.8	338.1	731.3
	Standard deviation	7.4	40.5	10.9	14.2	10.1	4.9	36.8	63.7

Fig. 11 shows the comparison of initial resistivity and stable resistivity of the investigated HPFRCs under different temperatures, including 0 °C (Fig. 11(a)), 25 °C (Fig. 11(b)), and 50 °C (Fig. 11(c)). For a temperature of 0 °C, as can be seen from Fig. 11a, compared with HPFRC1 series, the HPFRC0, HPFRC2, and HPFRC3 series generated an increase in initial and stable resistivity. For temperatures of 25 °C and 50 °C, as displayed in Fig. 11(b) and 11(c), compared with HPFRC1, the initial resistivity of HPFRC0, HPFRC2, and HPFRC3 exhibited a little difference, whereas the stable resistivity of HPFRC0, HPFRC2, and HPFRC3 produced a significant increase from 792.20/569.60 = 1.39 times (HPFRC3) to 935.00/569.60 = 1.64 times (HPFRC0) for 25 °C temperature, from 514.80/486.90 =

1.06 times (HPFRC2) to 731.30/486.90 = 1.50 times (HPFRC0) for 50 °C temperature. The clear reduction in stable resistivity of the HPFRC1 was thought due to the larger continuous spread of the embedded mono macro fibers inside the specimens, leading to decreasing the electrical polarization. The results of this study was consistent with that of the reference [12].

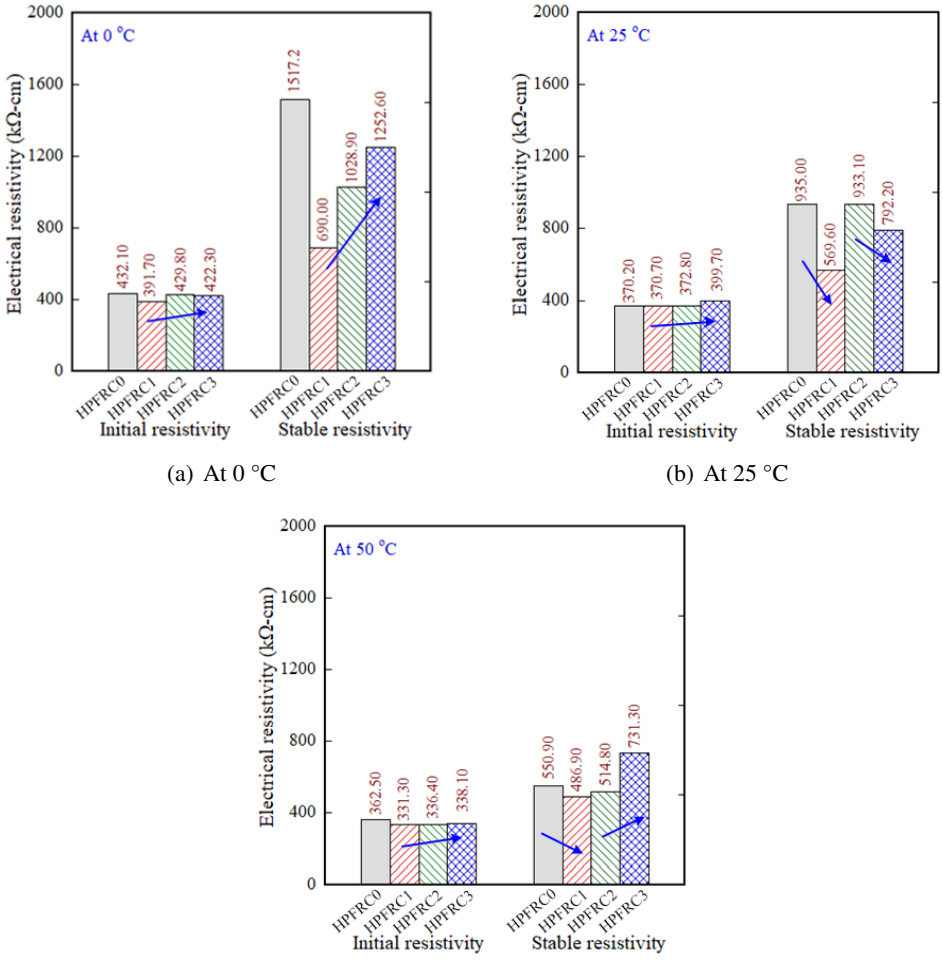

(a) At 0 °C

(b) At 25 °C

(c) At 50 °C

Figure 11. Comparative electrical resistivity of the studied HPFRCs

4.2. Effect of temperature on electrical resistivity of HPFRCs

Fig. 12 shows the effect of temperature on electrical resistivity of four studied HPFRCs: HPFRC0 (Fig. 12(a)), HPFRC1 (Fig. 12(b)), HPFRC2 (Fig. 12(c)), and HPFRC3 (Fig. 12(d)). As can be seen in Fig. 12, the electrical resistivity decreases with an increase in temperature from 0 °C to 50 °C regardless of HPFRC series. According to the explanation of Butera and Waldeck [22], the lower electrical resistivity of the studied HPFRCs, considered as a semiconductor material, was due to the more dopant atom density in HPFRCs at greater temperature. The study results of Nguyen et al. [15] and Kim et al. [16] also confimed the same trend of the electrical resistivity of HPFRCs with a change of temperature, i.e., there was a reduction in both initial and stable electrical resistivity with an increase of temperature varying from 15 to 35 °C and a constant relative humidity. Besides, the matrix with greater strength was observed to produce the greater electrical resistivity and polarization [16].

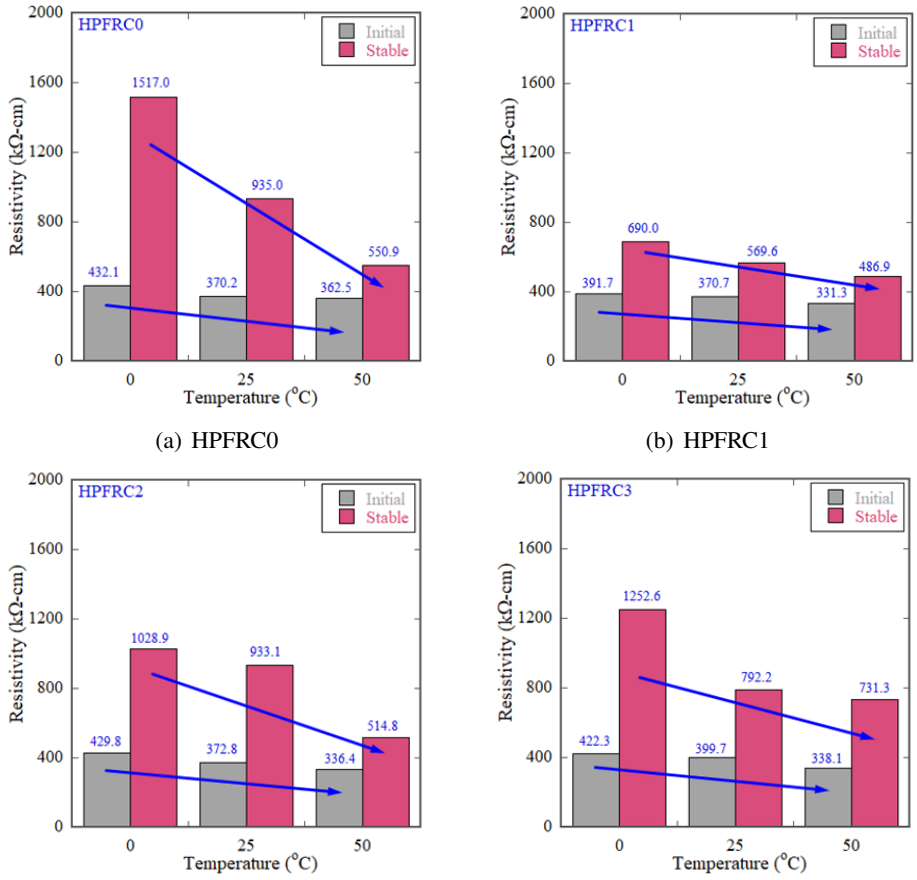

(a) HPFRC0 (b) HPFRC1

(c) HPFRC2 (d) HPFRC3

Figure 12. Effect of temperature condition on electrical resistivity of HPFRCs

5. Conclusions

The effect of temperature on electrical resistivity of high-performance fiber-reinforced concretes was investigated through an experimental study. Some derived conclusions could be listed from the research as follows:

- The electrical polarizations of the studied HPFRCs are more significant at the lower temperature. This is really one of considerable influencing factors in assessing self-sensing or self damage-sensing properties of HPFRCs.

- The electrical resistivity of HPFRCs obviously decreased with increasing of the temperature. The clear trend is useful in predicting the electrical resistivity of HPFRCs in natural enviroment, which is more conplex and uncontrolable, in comparison to laboratory enviroment.

- The initial electrical resistivity (at time of zero) of HPFRC was observed to be less sensitive to temperature than the 20-minute electrical resistivity.

- To develop the smart characteristic of self-sensing or self damage-sensing properties of HPFRCs, further investigation should be focused on the effect of fiber volume type and content on the electrical properties of HPFRCs at various temperatures and humidities.

Acknowledgements

The content in this research is a part of Master thesis of the author Phan Tan Duy, studying at Ho Chi Minh City University of Technology - Vietnam National University Ho Chi Minh City.

References

[1] Li, H., Ou, J. (2015). The state of the art in structural health monitoring of cable-stayed bridges. *Journal of Civil Structural Health Monitoring*, 6(1):43–67.

[2] Han, B., Ou, J. (2007). Embedded piezoresistive cement-based stress/strain sensor. *Sensors and Actuators A: Physical*, 138(2):294–298.

[3] Han, B., Yu, X., Ou, J. (2014). *Self-sensing concrete in smart structures*. Butterworth-Heinemann.

[4] Gupta, S., Gonzalez, J. G., Loh, K. J. (2016). Self-sensing concrete enabled by nano-engineered cement-aggregate interfaces. *Structural Health Monitoring*, 16(3):309–323.

[5] Hoheneder, J., Flores-Vivian, I., Lin, Z., Zilberman, P., Sobolev, K. (2015). The performance of stress-sensing smart fiber reinforced composites in moist and sodium chloride environments. *Composites Part B: Engineering*, 73:89–95.

[6] Naaman, A. E., Reinhardt, H. W. (1996). Characterization of high performance fiber reinforced cement composites—HPFRCC. In *High performance fiber reinforced cement composites*, volume 2, 1–24.

[7] Dhanapal, J., Jeyaprakash, S. (2019). Mechanical properties of mixed steel fiber reinforced concrete with the combination of micro and macro steel fibers. *Structural Concrete*, 21(1):458–467.

[8] Graybeal, B. (2007). Compressive Behavior of Ultra-High-Performance Fiber-Reinforced Concrete. *ACI Materials Journal*, 104(2):146–152.

[9] Nguyen, D.-L., Thai, D.-K., Ngo, T.-T., Tran, T.-K., Nguyen, T.-T. (2019). Weibull modulus from size effect of high-performance fiber-reinforced concrete under compression and flexure. *Construction and Building Materials*, 226:743–758.

[10] Tran, N. T., Pyo, S., Kim, D. J. (2015). Corrosion resistance of strain-hardening steel-fiber-reinforced cementitious composites. *Cement and Concrete Composites*, 63:17–29.

[11] Kim, D., Kang, S., Ahn, T.-H. (2014). Mechanical Characterization of High-Performance Steel-Fiber Reinforced Cement Composites with Self-Healing Effect. *Materials*, 7(1):508–526.

[12] Nguyen, D. L., Song, J., Manathamsombat, C., Kim, D. J. (2015). Comparative electromechanical damage-sensing behaviors of six strain-hardening steel fiber-reinforced cementitious composites under direct tension. *Composites Part B: Engineering*, 69:159–168.

[13] Song, J., Nguyen, D. L., Manathamsombat, C., Dong Joo, K. I. M. (2015). Effect of fiber volume content on electromechanical behavior of strain-hardening steel-fiber-reinforced cementitious composites. *Journal of Composite Materials*, 49(29):3621–3634.

[14] Nguyen, D.-L., Vuong, T.-N.-H., Nguyen, T.-T. (2017). Additional Carbon Dependent Electrical Resistivity Behaviors of High Performance Fiber-Reinforced Cementitious Composites. In *Lecture Notes in Civil Engineering*, Springer Singapore, 310–318.

[15] Nguyen, D.-L., Kim, D.-J., Thai, D.-K. (2019). Enhancing Damage-Sensing Capacity of Strain-Hardening Macro-Steel Fiber-Reinforced Concrete by Adding Low Amount of Discrete Carbons. *Materials*, 12(6): 938.

[16] Kim, M. K., Kim, D. J., An, Y.-K. (2018). Electro-mechanical self-sensing response of ultra-high-performance fiber-reinforced concrete in tension. *Composites Part B: Engineering*, 134:254–264.

[17] Chung, D. D. L. (2004). Electrically conductive cement-based materials. *Advances in Cement Research*, 16(4):167–176.

[18] Wittmann, F. H. (1973). Observation of an electromechanical effect of hardened cement paste. *Cement and Concrete Research*, 3(5):601–605.

[19] Wen, S., Chung, D. D. L. (2001). Carbon fiber-reinforced cement as a strain-sensing coating. *Cement and Concrete Research*, 31(4):665–667.

[20] Wen, S., Chung, D. D. L. (2001). Electric polarization in carbon fiber-reinforced cement. *Cement and Concrete Research*, 31(1):141–147.

[21] Chung, D. D. L. (2017). Cement-Matrix Composites. In *Carbon Composites*, Elsevier, 333–386.

[22] Butera, R. A., Waldeck, D. H. (1997). The Dependence of Resistance on Temperature for Metals, Semiconductors, and Superconductors. *Journal of Chemical Education*, 74(9):1090.